Cable Resistance in Spacecraft Deployable Mechanisms

Brian W. Schweinhart[1], Ziv A. Arzt[2], Brendan E. Nunan[3], Alex J. Mednick[4]
Physical Sciences, Inc., Andover, MA, 01810, USA

Nathan A. Pehrson[5], Ben Urioste[6]
Air Force Research Laboratory Space Vehicles Directorate, Kirtland AFB, NM, 87117, USA

The resistive torques of cable harnesses and service loops comprise a significant portion of the force budgets of deployable space mechanisms. The space engineering community lacks a reliable and methodical way to predict these forces early in the mechanism design process. Incumbent methods rely on estimates from heritage applications or use deployment prototype tooling. The latter approach is typically specific to the application and the design and therefore incurs timely and expensive iterations. This paper describes a methodology for directly predicting cable drag and resistive torque from the cable specification and deployment geometry alone. The method outlines a standard procedure for characterizing the elastoplastic and viscoelastic material properties of space cables. These experimentally-determined material properties are supplied along with deployed cable geometry to a FEA model, which predicts the cable resistive forces in a representative deployment system.

I. Nomenclature

AWG	=	American Wire Gauge
E	=	effective elastic modulus
FEA	=	Finite Element Analysis
K	=	strength coefficient
k_j	=	spring coefficient
l	=	element length
M	=	bending moment
n	=	strain hardening exponent
P	=	vertical tip load
PTFE	=	Polytetrafluoroethylene
PVC	=	Polyvinyl chloride
R	=	bend radius
x_N	=	tip horizontal position
y	=	distance to the neutral axis
α'	=	arc angle
Δt	=	time increment
ε	=	total strain

[1] Mechanical Engineer, Deployable Technologies, 20 New England Bus Center Dr., AIAA Member.
[2] Senior Engineer, Deployable Technologies, 20 New England Bus Center Dr., AIAA Member
[3] Senior Research Engineer, Deployable Technologies, 20 New England Bus Center Dr., AIAA Member
[4] Principal Engineer, Deployable Technologies, 20 New England Bus Center Dr., AIAA Member
[5] Senior Mechanical Engineer, Integrated Structural Systems, 3550 Aberdeen Ave SE, AIAA Member.
[6] Mechanical Engineer, Integrated Structural Systems, 3550 Aberdeen Ave SE, AIAA Member.

ε_y = total strain
η_j = damping coefficient
Θ = angle to the horizontal
σ = internal stress
σ_0 = stress of first sprint
σ_y = effective yield stress
τ_j = relaxation time

II. Introduction

The evolving scope of spacecraft missions has driven the need for larger, lighter deployable structures for solar panels, antennas, and other systems. Deployable spacecraft structures often include wires and cable harnesses connecting the deployed components to the satellite bus for power, RF signal, and data transmission. The cable harnesses directly influence the design of the deployment system as the cabling induces a significant resistive drag/torque that must be overcome by the deployment mechanism. The cables are defined by the power and signal needs of the spacecraft system to be deployed. Therefore, the large contribution (20-25%) to the deployment force budget remains fixed and must be determined as early as possible in the design process [1], [2]. Uncertainty in cable resistance torque will lead to heavy and overbuilt systems, since the initial cable drag forces must be overcome by sufficiently sized deployment actuators, which in turn are paired with comparably sized damping systems to prevent excessive impact forces at the end of motion. Typically, high uncertainty factors of at least 3.0 are given to wire harness torque values to mitigate the risk of excessive, unpredicted drag [3]. A model that provides a simple and accurate estimate of the resistive forces induced by wire harnesses would reduce costs by enabling space mechanism designers to more precisely predict cable drag loads and use lower force margin earlier in the design process.

The difficulty in accurately modeling electrical cables stems from the nonlinear elastic behavior of wires and insulation under stress, and that their mechanical behaviors are largely unexplored because they are not structural members [4]. Several research efforts [5], [6], [7] have looked at the mechanical response of long, narrow structures as their slenderness allows for the significant simplification from a three-dimensional model to a one-dimensional model. These models often represent slender structures in a wide range of situations: bending, twisting, shearing, tension, and compression. Previous research [7] that has attempted to define the material properties for long, slender objects, have largely done so through tests that mimic conditions of structural cables, i.e. tension and torsion. Because wire harnesses in deployable space systems experience predominantly bending loads, their effective material properties are best defined by a basic bending test. A cantilever bending test is both simple and representative of wire movement in application. An analytical model of the cables can then be developed from the results of the bending test.

Although similar in shape and manufacturing method to structural cables, most electrical wires are composed of a highly ductile copper conductor surrounded by a thermoplastic insulation. The softness of their insulation and the relatively small diameter of the conductor means the non-linear material properties of the insulation dominate and the mechanical behavior is challenging to characterize. Furthermore, space-rated electrical wires often include multiple layers of protective insulation, with complex load paths due to being bundled and wrapped in plastic insulation. When electrical wires are induced with a bending force, their response closely follows that of an elastoplastic material (seen in Fig. 1). Elastoplastic materials are characterized by two specific sections of their stress-strain curve [8]. An elastic zone below the yield strength followed by a plastic zone where strain hardening and permanent deformation occur.

Electrical cables for space systems are typically stored in bent positions for weeks or months before launch, leading to creep effects that are not observed in a recently bent wire. Relaxation and creep are types of viscoelastic deformation behavior. When placed under stress, many polymers and some metals change shape over time. The initial, elastic deformation becomes permanent as the material's internal structure flows in a phenomenon known as stress relaxation. Stress relaxation increases the resistive cable drag force during deployment because the cable relaxes into its bent position, and more plastic strain must be overcome in order to complete the deployment after the stress relaxation occurs. It is therefore critical to include stress relaxation in the cable drag model, because neglecting the viscoelastic properties of the wire would lead to a non-conservative cable drag force prediction.

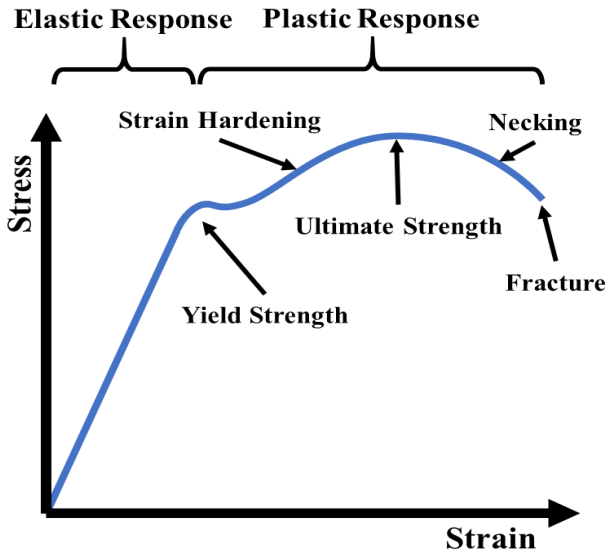

Fig. 1 Stress-strain curve for an elastoplastic material.

In this work, we propose a methodology for predicting the resistive torque that a single-core electrical cable produces on a basic service loop seen in deployment space systems. We developed an analytical cable bending model alongside a cantilever bending test apparatus to characterize the material properties. We also included a viscoelastic model in the material characterization to capture creep effects. To capture the response of the wires in an exemplar deployment system, we designed a second test apparatus representative of typical deployable space structures. We developed a corresponding FEA model alongside this test system to predict the deployment torque of the service loop, with a target error margin of 10%. This error margin was defined from error obtained in the results by previous work on modeling the force response of similar wires [4]. While the error goal is similar, we added viscoelastic effects and a representative service loop test. We showed that the process defined in the following sections obtains the effective material properties of a wire and model its response in a representative service loop within the aforementioned error.

III. Methodology

Our methodology for predicting cable drag begins with a standardized test for determining the homogenized, effective elastoplastic and viscoelastic material properties of single cables. During this process, the parameters of the constitutive material models that describe the cables/harnesses are iteratively calibrated to experiment using an Euler-Bernoulli beam bending model. The calibrated material properties then serve as inputs along with the geometry to FEA and analytical predictive models, a process built on prior work done in [4]. We replicated the cantilever bending experiment and expanded upon the material property definition process and the constitutive model to include creep phenomenon.

Furthermore, we developed a two-panel deployment system that serves as a validation test-bed for the material characterization test. The two-panel deployment experimental test-bed replicates a simple service loop seen in space deployment applications, i.e. solar panels or antenna arrays. The setup records the torque a wire in a service loop produces and serves as a validation tool against an FEA model of the deployment using the effective material properties. The full methodology is depicted below in Fig. 2.

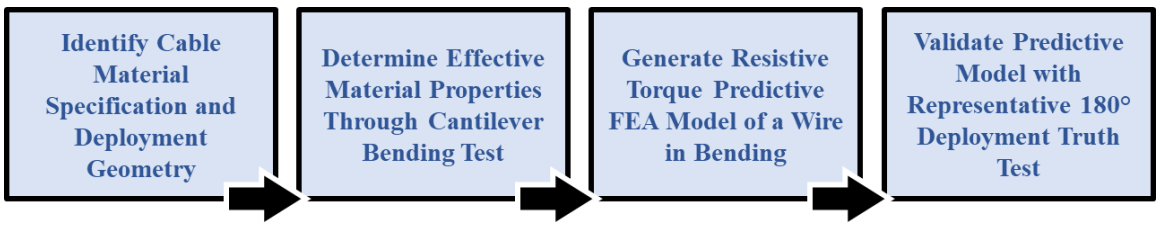

Fig. 2 Methodology flow for finding the force response of wires in a deployment system.

IV. Characterizing Wire Material Properties

The process to characterize the material properties of electrical cables with a cantilever bending test is performed in three steps, as laid out in this section. (A) A cantilever bending apparatus is used to capture the force-deflection response of the cables under investigation. (B) Constitutive material models are used with a beam bending model to simulate the force-deflection response of the cables under investigation. (C) An optimization algorithm is used to calibrate the material properties in the beam bending model to the experimental results.

A. Experimental Cantilever Beam Bending Setup

A standardized cable bending apparatus was used in order to generate the experimental force vs. deflection curves for material property fitting. The apparatus was adapted from prior research [4], and works by testing cantilevered, segments of wire. This apparatus is consistent with the beam bending model described above, and was selected in order to derive the material properties to be used in that model, which are then applied to general FEA models.

The apparatus bends the wire by holding one end fixed to a linear actuator, and tying a string on the other end up to a force sensor held above the test specimen, as depicted in Fig. 3. The linear actuator deflects the wire downward, creating a bend in the wire. Adjusting the deflection distance and the length of the wire affects the strain level of the bend. For example, an 80 mm long 16 AWG wire deflected 50 mm will have a strain of around 4%, but the same gauge wire with a length of 55 mm will have a strain of 15% with a similar deflection distance. A 55 mm length wire was used to match the largest strain seen in the service loop deployments. A force sensor, displacement sensor, and camera recorded the wire's mechanical response simultaneously at 10 Hz. To capture viscoelastic effects, we edited the motion control software to add time delays after max deflection and recorded the wire's force response at intervals up to 16 hours.

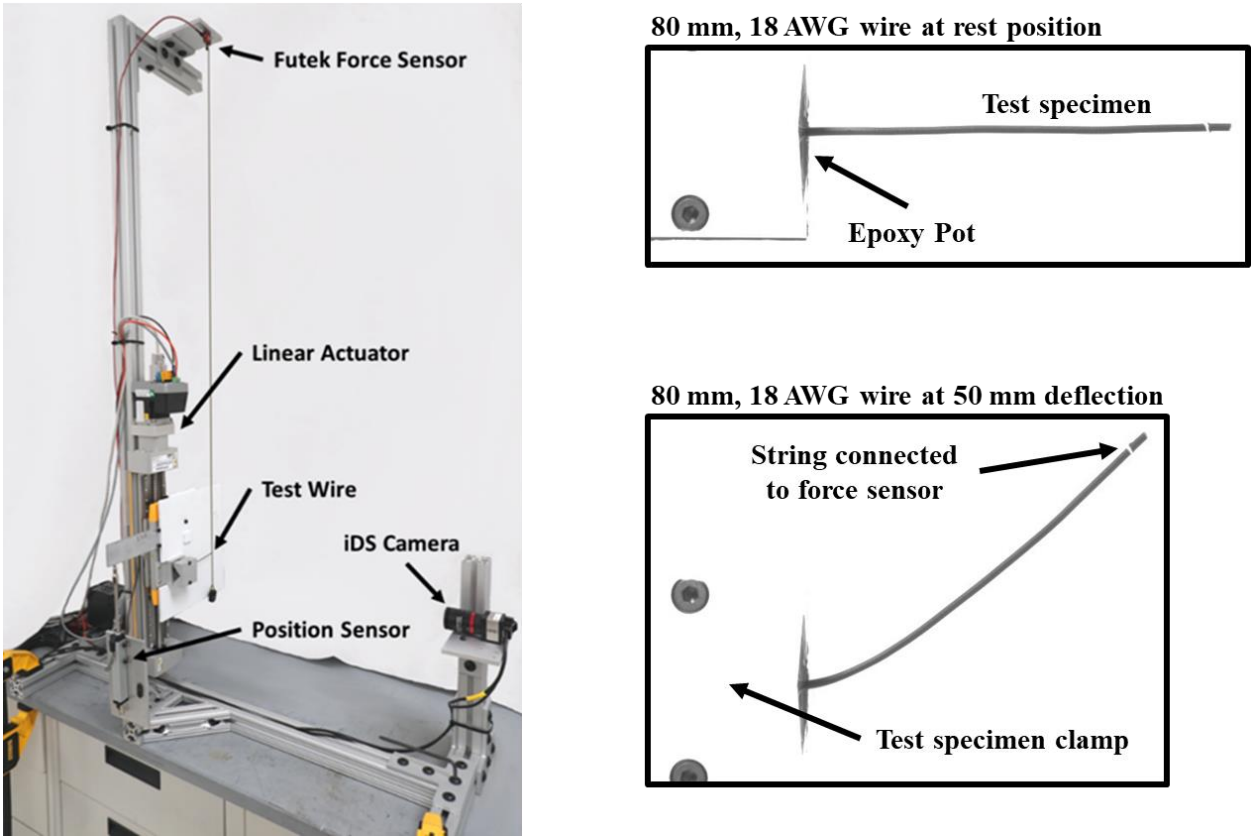

Fig. 3 Overview of the experimental test apparatus, and captured images filtered black and white from an experimental test.

B. Analytical Cable Bending Model

We created a cantilever beam bending model in order to determine the effective homogeneous wire material properties that best fit the experimental results. The model discretizes the wire into elements of equal length. Shear

and axial deformation are neglected and each element is assumed to be in pure bending. As previously mentioned, wires in space applications are commonly placed in service loops that predominantly experience bending loads; therefore, it is appropriate to make this pure bending assumption. Under the pure bending load, the individual elements take the shape of circular arcs. Because axial deformation is neglected, the arc length of each element remains constant over the simulation. The radius of curvature of each element is dependent on the internal bending moment, which is evaluated at the midpoint of each element and held constant through the length of the element.

Each element has four unknowns that are solved for using a corresponding set of four non-linear equations. The kinematics are summarized in Fig. 4. The unknowns are the *X* and *Y* position of the nodes on the right hand side of each element, the arc angle α' that the element spans, and the internal bending moment *M* in the element. The *X* and *Y* locations for each element can be determined based on the kinematics using the assumption that the arc length of the element remains constant:

$$X_i = X_{i-1} + \frac{l_i}{\alpha_i'}\sin(\alpha_i')\cos(\theta_{i-1}) - \frac{l_i}{\alpha_i'}(1-\cos\alpha_i')\sin(\theta_{i-1}) \tag{1}$$

$$Y_i = Y_{i-1} + \frac{l_i}{\alpha_i'}\sin(\alpha_i')\sin(\theta_{i-1}) + \frac{l_i}{\alpha_i'}(1-\cos\alpha_i')\cos(\theta_{n-i}) \tag{2}$$

Where l_i is the length of the element and θ_{i-1} is the angle that the previous element forms with the global horizontal axis. The angle with the horizontal θ_i for each element can be calculated recursively as $\theta_i = \theta_{i-1} + \alpha_i'$.

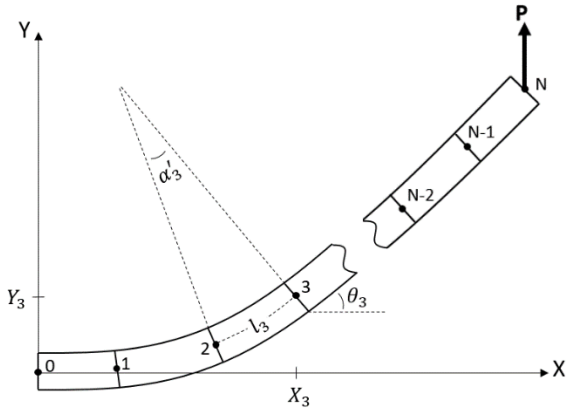

Fig. 4 Kinematics for the beam bending model.

For the cantilever geometry, the internal bending moment for each element *M* is the cantilever tip load multiplied by the horizontal distance between the midpoint of the element and the cantilever tip. The bending moment is calculated as follows:

$$M_i = P\left[X_N - \left(X_{i-1} + \frac{l_i}{\alpha_i'}\sin\left(\frac{\alpha_i'}{2}\right)\cos(\theta_{i-1}) - \frac{l_i}{\alpha_i'}\left(1-\cos\left(\frac{\alpha_i'}{2}\right)\right)\sin(\theta_{i-1})\right)\right] \tag{3}$$

Where P is the vertical tip load and X_N is the horizontal position of the tip of the cantilever beam.
The constitutive material model relates the arc angle α' of each element to the internal bending moment. The internal bending moment is calculated as follows:

$$M_i = \int_A \sigma\, y\, dA \tag{4}$$

Where σ is the internal stress, *y* is the vertical distance to the neutral axis of the cross-section, and the integral is taken over the cross-sectional area of the wire. For symmetric cross sections, the neutral axis is located in the middle of the cross section.

The constitutive material laws define the stress as a function of strain and the load history. Two different constitutive material laws were considered to model the elastoplastic and viscoelastic response of the cable. Adopting a strain hardening exponent law from past research in [4], the elastoplastic response was modeled as follows:

$$\sigma_{elastoplastic} = \begin{cases} E\varepsilon & if\ \sigma < \sigma_y \\ \sigma_y + K\left(\varepsilon - \varepsilon_y\right)^n \end{cases} \tag{5}$$

Where E is the effective elastic modulus of the material, ε is the total strain, σ_y is the effective yield stress, K is the strength coefficient, ε_y is the yield strain calculated as $\varepsilon_y = \sigma_y/E$, and n is the strain hardening exponent. Note that the elastoplastic model is independent of the load rate and load history.

A generalized Maxwell model was used to model the viscoelastic response of the cable. The generalized Maxwell model assumes that the stress in the material can be approximated as a set of linear springs and dashpots, as shown in Fig. 5. The viscoelastic stress state at each time step can be calculated numerically as follows [9]:

$$\sigma^t{}_{viscoelastic} = k_0\varepsilon^t + \sum_{j=1}^{J} \mathrm{h}_j^t, \quad \text{where}$$

$$\mathrm{h}_j^t = \exp\left(-\frac{\Delta t}{\tau_j}\right) h_j^{t-1} + \left(\frac{k_j}{k_0}\right) \frac{1 - exp\left(-\frac{\Delta t}{\tau_j}\right)}{\frac{\Delta t}{\tau_j}} (\sigma_0^t - \sigma_0^{t-1}) \tag{6}$$

Where k_j are the spring coefficients, η_j are the damping coefficients, τ_j are the relaxation times calculated as $\tau_j = \eta_j/k_j$, and Δt is the time increment. σ_0 is the stress response of the first spring, which is calculated as $\sigma_0 = \varepsilon\mu_0$. The viscoelastic model depends on both the load rate and load history.

The full stress response of the wire is the sum of the elastoplastic and viscoelastic components:

$$\sigma = \sigma_{elastoplastic} + \sigma_{viscoelsatic} \tag{7}$$

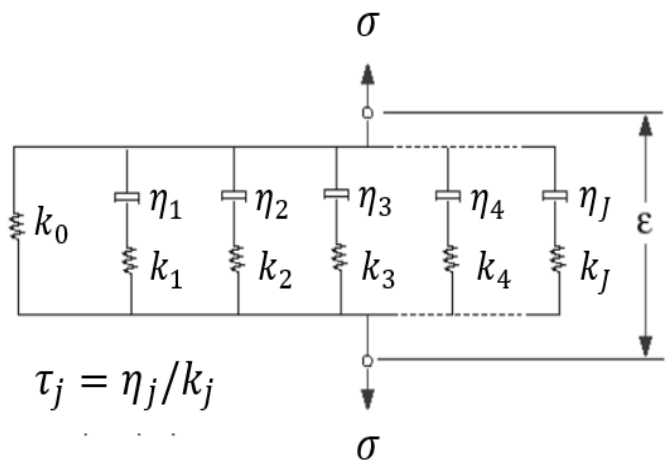

Fig. 5 Generalized Maxwell model for viscoelasticity.

The strain at each point on the cross-section depends on the distance from the neutral axis y as well as the bend radius R of the element. For a beam in pure bending, $\varepsilon = y\alpha_i'/l_i$.

The internal bending moment at each time step can be computed by substituting Eqs. (5-7) into Eq. (4), and numerically integrating over the cross-section of each element. Eqs. (1-4) then provide the set of 4*N coupled non-linear equations that can be solved simultaneously to determine the unknown displacements, angles and internal bending moments for each element. The boundary conditions used in Eqs. (1-3) for the first element are $X_0 = Y_0 = \theta_0 = 0$.

The elastoplastic and viscoelastic stresses are calculated separately and then superimposed to preserve the connection to commercial FEA software. The material parameters used by the analytical bending models can be entered into the established plasticity and viscoelasticity material models used in commercial FEA software in order

to simulate more complex bending load cases in three dimensions. The two material models can be superimposed in any commercial FEA software by creating two identical meshes, bonding all of the overlapping nodes and assigning one material model to each of the meshes.

C. Optimization Algorithm

The material properties needed for the model were derived using a gradient-based, interior-point optimization method to most closely match the experimental results for a given cable sample. The inputs to the optimization were an experimental cantilever force vs. deflection curve, as well as the geometry of the cantilever sample. The optimization adjusted the material model input parameters with each objective function evaluation in order to minimize the RMS error between the analytical bending model and the experimental results.

The number of design variables (i.e. material parameters to be determined) in the optimization were reduced by holding several of the parameters constant. In accordance with [4], the elastic modulus and yield stress were calculated prior to the optimization for each sample by assuming that yield first occurs at 5% of the cantilever tip deflection. In addition, the time constants for the viscoelastic model were fixed prior to the optimization. As a result, the optimization algorithm only needed to solve for $2 + J$ material constants, where two of the constants come from the elastoplastic model (K, n), and J is the number of spring-damper pairs in the viscoelastic model.

V. Representative Deployment System

The team designed and built a second test apparatus to test wires in a service loop on a representative two-panel deployment system, pictured in Fig. 6. The system connected to a 4000 series Instron machine, which provides linear motion and records force and displacement data. Four precision hinges coupled the two panels to convert the linear motion of the Instron machine to angular motion of deploying panels. We added margin to the min and max limits of the panel deployment to prevent the Instron from moving past the mechanical limits of the panel assembly. Due to these limits, the full deployment motion was limited from 6° to 154°. Clamps held the wires to the panels during the deployment motion, and they held the service loop in a plane perpendicular to the panels. The service loop was formed by wrapping the wires around mandrels of a radius ten times the outer diameter of whichever wire was being tested. We chose this service loop size from NASA's workmanship standards on wire harnesses. The optimal bend radius for wires size 10 AWG or smaller is 10 x OD [10].

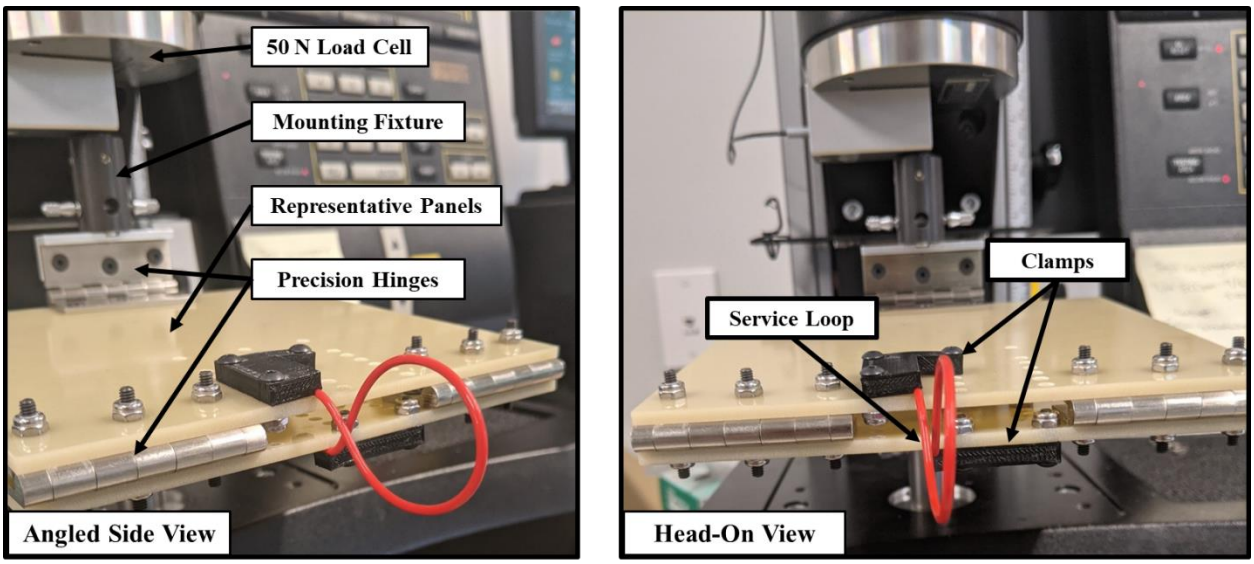

Fig. 6 Overview of the two-panel validation test apparatus.

To find just the deployment torque of the wire, we first tested the two-panel system without cables attached. Multiple stow and deploy tests were run to capture the response of the empty panels. We averaged the results of these tests to develop a baseline response of the empty panels that was then subtracted from the later results with the cables attached. The process for mounting the wire on the panel was completed with the two-panel system open to the max deployment angle. We first clamped one end of the wire to one panel, formed the service loop, and then clamped the other end of the wire to the second panel. Once clamped, the team visually verified that the service loop was properly

aligned on the panels as significant misalignment could have led to an undesirable motion of the service loop. The panel system was then placed into the Intron machine at the same open position during the setup. We first ran the retraction test, closing the two-panel system to the "stowed" state of 6°, capturing the force and displacement of the panels through its motion. Next, we ran the deployment test to open the panels to a limit of 154° (limited by geometry of the test apparatus with 3° margin). This deployment test is depicted in Fig. 7. Force and displacement data were again captured for this test.

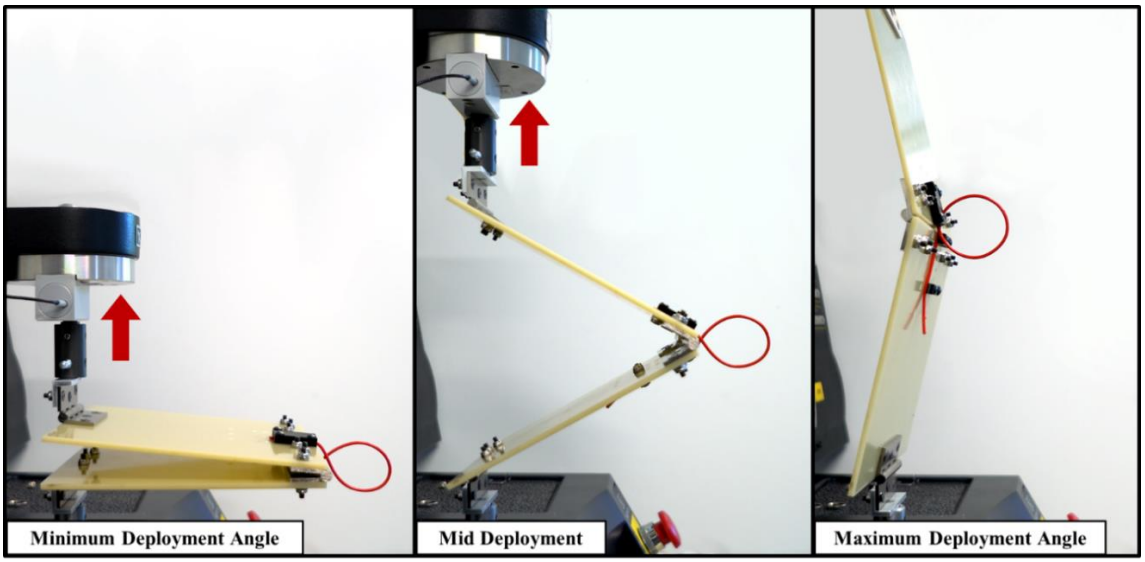

Fig. 7 Captured images of the deployment test of the two-panel validation test apparatus.

A quarter-symmetry, quasi-static, 3D FEA model was used to predict the torque vs. deflection profile for the service loop. The boundary conditions and load steps of the FEA model are described in Fig. 8. The model used a bonded contact between the flexible cable and a rigid panel. The three degrees of freedom for the panel were controlled by prescribing the x displacement at one point, and both the x and y displacements at another point on the panel. The symmetry condition in the middle of the service loop fixed the cable vertically but allowed it to slide horizontally.

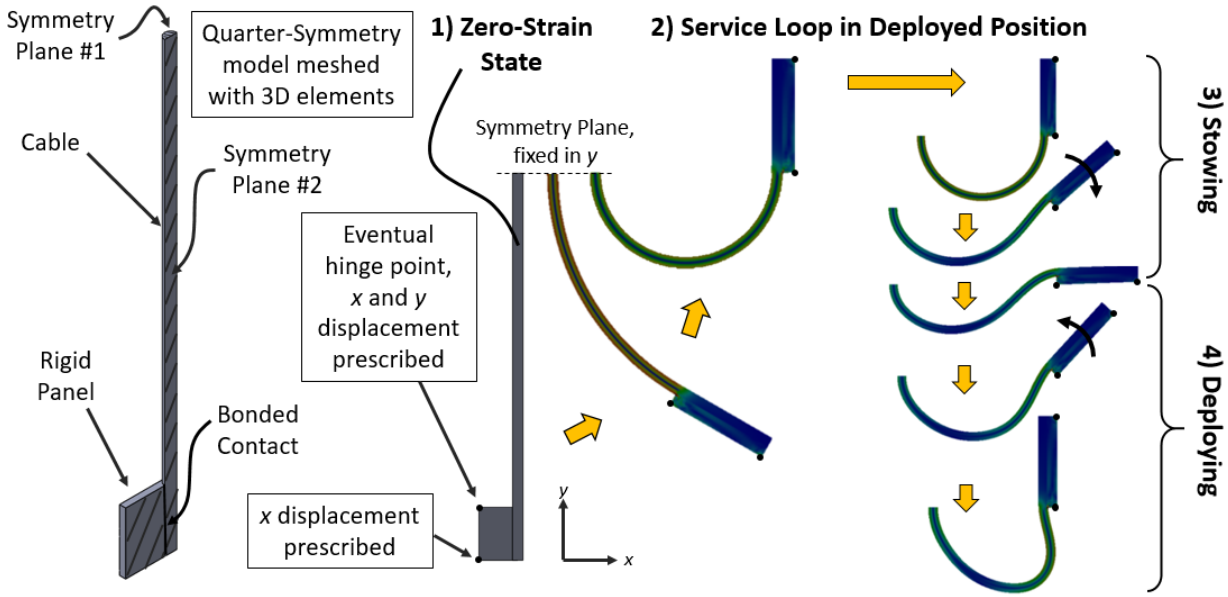

Fig. 8 Boundary conditions and load steps for the service loop FEA model.

The simulation starts with the wire at its zero strain state in a straight position. During the first part of the simulation, the wire is bent into a service loop configuration with the panels in the fully deployed position. Next, the wire is subjected to several stow and deploy cycles. The resistive torque is calculated using the reaction forces at the constrained points on the panel.

VI. Material Characterization and Representative Deployment Results

Results for four wires are presented in this paper. These wires are a 16 AWG PTFE, 20 AWG PTFE, 18 AWG PVC, and 20 AWG PVC. All of the wires tested in this work had solid cores. A cantilever test stand was used to characterize the effective material properties of the wires in bending. A short 55 mm cantilever span was selected in order to achieve the high strains observed in service loop applications. The cantilever tip deflection was set to 45 mm at a rate of 2.25 mm/s for all samples.

Best-fit properties for each sample were first calculated using the elastoplastic material model with no viscoelastic terms. Fig. 9 shows the experimental force vs. deflection along with the best-fit 1D elastoplastic model results. Table 1 summarizes the elastoplastic material coefficients for the wires.

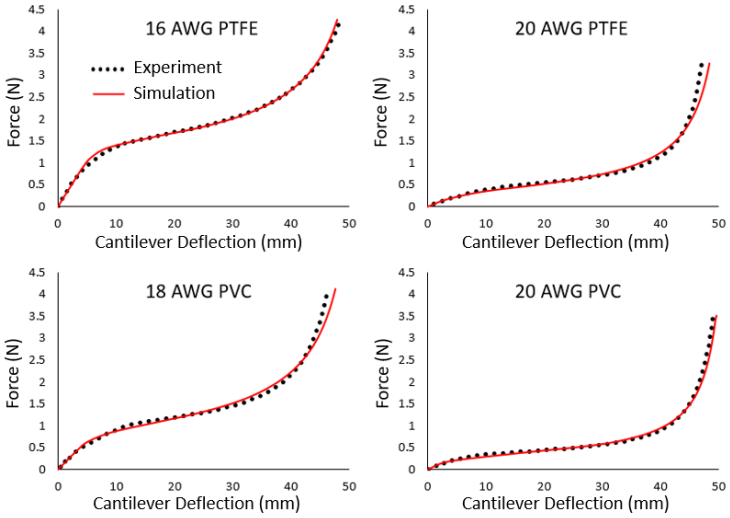

Fig. 9 Force vs. deflection experimental results and best fit simulation results for 16 AWG PTFE, 20 AWG PTFE, 18 AWG PVC and 20 AWG PVC wires.

Table 1 Effective elastoplastic material properties for solid core wire samples.

Wire Sample	Diameter (mm)	E (MPa)	σ_y (MPa)	K (MPa)	n	Fit Error %
16 AWG PTFE	2.00	14800	42.2	55.5	0.27	0.8%
20 AWG PTFE	1.55	10030	20.5	586.0	0.73	2.19%
18 AWG PVC	3.10	1620	6.73	32.6	0.52	2.15%
20 AWG PVC	2.60	1305	4.81	109.6	0.99	1.28%

The FEA service loop deployment simulations using the best-fit elastoplastic material properties were able to predict the experimental response within 10% for deployment angles less than 120°. Fig. 10 shows the simulated and experimental torque vs. deflection profile for the 16 AWG PTFE wire. Negative torque values indicate a service loop torque aiding the panels in opening, while a positive value indicates torque holding them shut.

The experimental results diverge from the service loop simulation for deployment angles above 120°. An analytical model of the joint forces showed that the difference in torque at high deployment angles can be attributed to increased joint friction caused by the presence of the service loop. We designed the system with nickel precision butt hinges to reduce play in the system and improve repeatability, but the hinges were not made from low friction materials nor oiled. More accurate results at higher deployment angles could be obtained using lower friction hinges or flexures, and these adjustments can be made for future experiments. While the intent of this work is to quantify the resistive torque of the cable alone, the result highlights that hinge friction should be considered in conjunction with the service loop resistive torque during the design process of deployable structures in space applications.

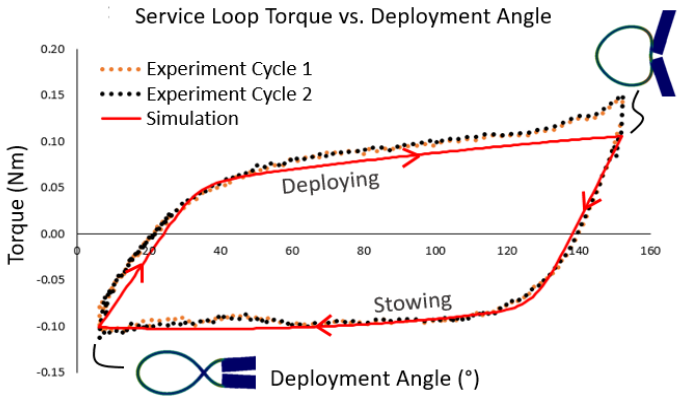

Fig. 10 Torque vs. deployment angle experimental and simulation results for 16 AWG PTFE wire with a 20 mm diameter service loop.

After determining the effective elastoplastic material properties based on cantilever tests and verifying that the service loop torque predictions matched the experimental results, we fit the hybrid elastoplastic-viscoelastic material model to the 16 AWG PTFE wire sample. We experimentally characterized the relaxation of the wire in bending using a deflect-and-hold test on the cantilever test stand. After deflecting to 45 mm at a rate of 2.25 mm/s, the tip of the cantilever tip was held at the 45 mm deflection for 40 hours. The force was measured by the load cell at a sampling rate of 1 Hz.

Experimental results along with the best-fit material model are shown in Fig. 11Fig. 11. A viscoelastic model with five spring/damper pairs was able to produce a fit within 4% of the experimental results. The five time constants were fixed at 1, 10, 100, 1000 and 10000 seconds, and the spring constants for each spring/damper pair were tuned to produce the best fit results. The elastoplastic-viscoelastic material constants are summarized in Table 2. Note that because the viscoelastic and elastoplastic material models are acting in parallel, inclusion of the viscoelastic terms changes in the elastoplastic constants from the case where the elastoplastic model was run alone.

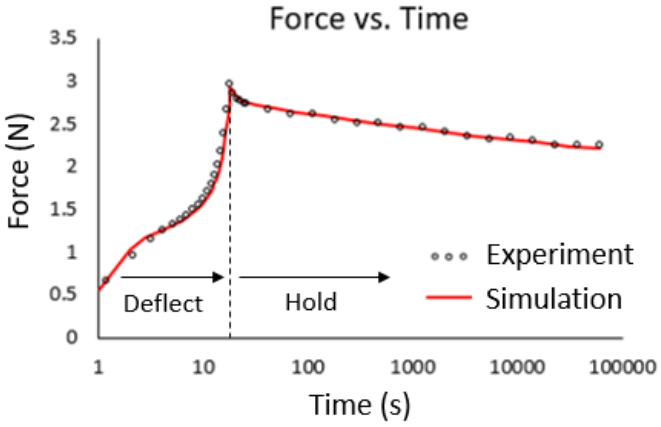

Fig. 11 Best fit viscoelastic-elastoplastic material model for a deflect-and-hold cantilever test on the 16 AWG PTFE wire sample.

Table 2 Best fit viscoelastic constants for 16 AWG PTFE wire.

Material Model	E (MPa)	σ_y (MPa)	K (MPa)	n	k_1 (MPa) τ=1	k_2 (MPa) τ=10	k_3 (MPa) τ=100	k_4 (MPa) τ=1000	k_5 (MPa) τ=10000
Viscoelastic-Elastoplastic	15690	39.8	21.2	0.29	300	50	50	50	50

Fig. 12 shows a service loop simulation that was run with both the elastoplastic-only and the elastoplastic-viscoelastic material models. A 24 hour rest period was added with the cable in the fully stowed position in order to study the impact of relaxation. Relaxation accounted for a 26% decrease in deployment aiding torque at the stowed

position, which corresponds well to the 24% drop in force during the cantilever test. During the 15 second duration deployment motion, the elastoplastic-viscoelastic model relaxed back towards the elastoplastic-only model, and the maximum torque ended only 4% above the elastoplastic model. This result was expected because a majority of the relaxation occurred early on, in the first 100 seconds of the cantilever test. While a full elastoplastic-viscoelastic model can be constructed to study the behavior of the service loop in detail, the results also show that a brief analysis of the cantilever deflect-hold relaxation test can yield a great deal of insight on how the service loop will respond.

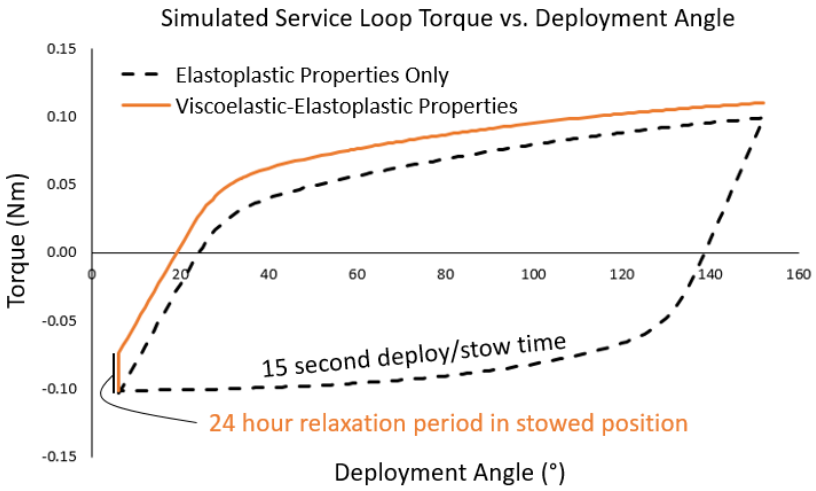

Fig. 12 Comparison of service loop torque vs. deployment angle for the elastoplastic-only and elastoplastic-viscoelastic material models.

VII. Conclusion

The authors have developed a methodology for defining the force response of cabling in space mechanism deployment systems. A 1D nonlinear elastoplastic and viscoelastic model was created to characterize the response of the wires under cantilever bending. The 1D model was used in conjunction with experimental test data to determine the best-fit effective material properties for the cable samples. The best-fit properties were used in a finite element simulation to predict the resistive torque response of the wire in a representative two-panel deployment application. Results showed the predicted force response met the goal of less than 10% error relative to the experiment.. The work described in this paper offers a reliable and repeatable method to predict the response of simple electrical cables in service loops. These results show a potential of time and cost reduction in designing deployment systems through minimizing the margin in deployment torque by reducing uncertainty in wire harnesses.

The 1D model developed in this work does not rely on commercial FEA software, making the material parameter fitting process more accessible to the wider space community. For example, the simplified model could allow a test center to measure and characterize the material properties for a broad number of cable samples in order to quickly build a database at a lower cost. At the same time, the best fit properties that come out of the model can still be used directly in FEA simulations to analyze more complex cabling configurations, such as bundles, coaxial cables, fiber optic cables, and ribbons. The methodology for finding the effective material properties would remain similar to the methodology laid out in this paper. The FEA model would be expanded to include the more complex interaction between multiple wires in a bundle, or multiple material layers seen in coaxial cables.

The next steps beyond the work defined in this paper would be testing more complex and unique cables to expand the constitutive model. Furthering the predictive model with expanded testing and a machine learning algorithm would offer more accurate estimates to the resistive torque of wire harnesses on hinge-line deployment systems. Furthermore, the predictive FEA simulation can be used to model a larger variety of deployment setups, from large angle rotations to unique multi-joints in complex structures. This model could be furthered even more by accounting for the thermal environment of space and capturing the response of wires subject to extreme temperatures.

Acknowledgement of Support and Disclaimer

This material is based upon work supported by United States Air Force under Contract Number FA9453-19-C-0006. Any opinions, findings and conclusions or recommendations expressed in this material are those of the author(s) and do not necessarily reflect the views of United States Air Force.

References

[1] Aglietti, G. S., "Current Challenges and Opportunities for Space Technologies," *Frontiers in Space Technologies,* vol. 1, p. 1, 2020.

[2] Calassa, M. C. and Kackley, R., "Solar Array Deployment Mechanism," *NASA. Johnson Space Center, The 29th Aerospace Mechanisms Symposium,* 1995.

[3] Lee, K., "Solar array deployment qualification for the LMX of buses," *Proceedings of the 11th European Space Mechanisms and Tribology Symposium,* vol. 591, pp. 225-233, 2005.

[4] G. &. U. P. Labruyère, "ESA mechanisms requirements," in *Sixth European Space Mechanisms and Tribology Symposium*, Zürich, 1995.

[5] Taghipour, E., Vemula, S. S., Wang, Z., Zhou, Y., Qarib, H., Gargesh, K., Headings, L. M., Dapino, M. J. and Soghrati, S., "Characterization and computational modeling of electrical wires and wire bundles subject to bending loads," *International Journal of Mechanical Sciences,* vol. 140, pp. 211-227, 2018.

[6] Foti, F. and Martinelli, L., "Mechanical modeling of metallic strands subjected to tension, torsion and bending," *International Journal of Solids and Structures,* vol. 91, p. 17, 2016.

[7] We, W. and Cao, X., "Mechanics model and its equation of wire rope based on elastic thin rod theory," *Internation Journal of Solids and Structures,* Vols. 102-103, p. 9, 2016.

[8] Ghoreishi, S. R., Cartraud, P., Davies, P., and Messager, T., "Analytical modeling of synthetic fiber ropes subjected to axial loads. Part I: A new continuum model for multilayered fibrous structures," *International Journal of Solids and Structures,* vol. 44, no. 9, p. 19, 2007.

[9] Kossa, A., "Exact stress integration schemes for elastoplasticity," Budapest University of Technology and Economics Department of Applied Mechanics, 2011.

[10] Kaliske, M.. and Rothert, H., "Formulation and implementation of three-dimensional," *Computational Mechanics,* vol. 19, pp. 228-239, 1997.

[11] National Aeroanutics and Space Administration, *Workmanship standard for crimping, interconnecting cables, harnesses, and wiring,* 2016.

[12] Jones, R. M., *Mechanics of Composite Materials,* CRC Press, 1998.